iScience

CellPress
OPEN ACCESS

Perspective

Toward next-generation fuel cell materials

M.A.K. Yousaf Shah,[1] Peter D. Lund,[1,2,*] and Bin Zhu[1,*]

SUMMARY

The fuel cell's three layers—anode/electrolyte/cathode—convert fuel's chemical energy into electricity. Electrolyte membranes determine fuel cell types. Solid-state and ceramic electrolyte SOFC/PCFC and polymer based PEMFC fuel cells dominate fuel cell research. We present a new fuel cell concept using next-generation ceramic nanocomposites made of semiconductor-ionic material combinations. A built-in electric field driving mechanism boosts ionic (O^{2-} or H^{+} or both) conductivity in these materials. In a fuel cell device, non-doped ceria or its heterostructure might attain 1 Wcm^{-2} power density. We reviewed promising functional nanocomposites for that range. Ceria-based and multifunctional semiconductor-ionic electrolytes will be highlighted. Owing to their simplicity and abundant resources, these materials might be used to make fuel cells cheaper and more accessible.

INTRODUCTION

The principle of a fuel cell was introduced by Sir William Grove already in 1839 who showed that an electric current could be produced from an electrochemical reaction between hydrogen and oxygen over a coupled catalyst electrode[1] shown in the historical Figure 1.

The fuel cell (FC) development since Grove's invention has followed the same kind of structural design in which the FC composes of three functional components: The anode, electrolyte, and cathode, which is also called the membrane electrode assembly (MEA).[2,3] The core component of the fuel cell is the electrolyte which also defines the type of the fuel cell and its operational temperatures. Accordingly, the most common fuel cell types are the solid oxide fuel cell (SOFC), proton ceramic fuel cell (PCFC), molten carbonate fuel cell (MCFC), phosphorus acid fuel cell (PAFC), polymer electrolyte membrane fuel cell (PEMFC), and alkaline fuel cell (AFC) also shown in Figure 2. Their operational temperatures are as follows: SOFC: 800–1000°C, PCFC: 600–800°C, MCFC: 600–650°C, PAFC: 120–220°C; PEMFC: 20–220°C and AFC: 20–120°C.[4–6] Good fuel cell efficiency can be reached without noble metal catalysts at a high temperature, e.g., 600–1000°C. This would be necessary for low-temperature fuel cells (<300°C) to achieve good performance.

Owing to the electrolytes' properties, the temperature range between 300-600°C is not well covered. The temperature levels shown here represent typical electrolyte materials and ionic conductivities to deliver sufficiently high-power density. Advanced thin-film manufacturing technologies for SOFC or PCFC enable making thinner electrolytes with lower resistance, thus reducing the fuel cell operating temperatures well below those above, e.g., in PCFC to 500°C.[7,8]

In addition, each fuel cell type employs a specific variety of ions in the transport process in the electrolyte: SOFC (O^{2-}), MCFC ($CO_3^{=}$), AFC (OH^{-}), and protons in PCFC, PAFC, and PEMFC as demonstrated in Figure 2.

Targeting the 300–600°C temperature range for fuel cell operation would require seeking electrolytes beyond the traditional sphere. Still, oxygen-ion conductors could be relevant in this context.[9] Figure 3 shows a range of oxide materials of interest that could potentially replace the conventional high-temperature yttria-stabilized zirconia (YSZ) electrolyte used in SOFC[10–15] but still missing a high enough ionic conductivity (>0.1 S/cm) at a temperature below 600°C. Proton-conducting ceramic electrolytes $BaZrO_3$ and $BaCeO_3$ have recently been identified as promising materials for PCFC,[16–18] their ionic conductivities remain at 10^{-3}-10^{-2} S/cm only at 600°C.[15]

[1]Jiangsu Provincial Key Laboratory of Solar Energy Science and Technology/Energy Storage Joint Research Center, Southeast University, Nanjing, Jiangsu, China

[2]New Energy Technologies Group, Department of Applied Physics, Aalto University School of Science, P. O. Box 15100, 00076 Aalto, Espoo, Finland

*Correspondence: zhu-bin@seu.edu.cn (P.D.L.), peter.lund@aalto.fi (B.Z.)

https://doi.org/10.1016/j.isci.2023.106869

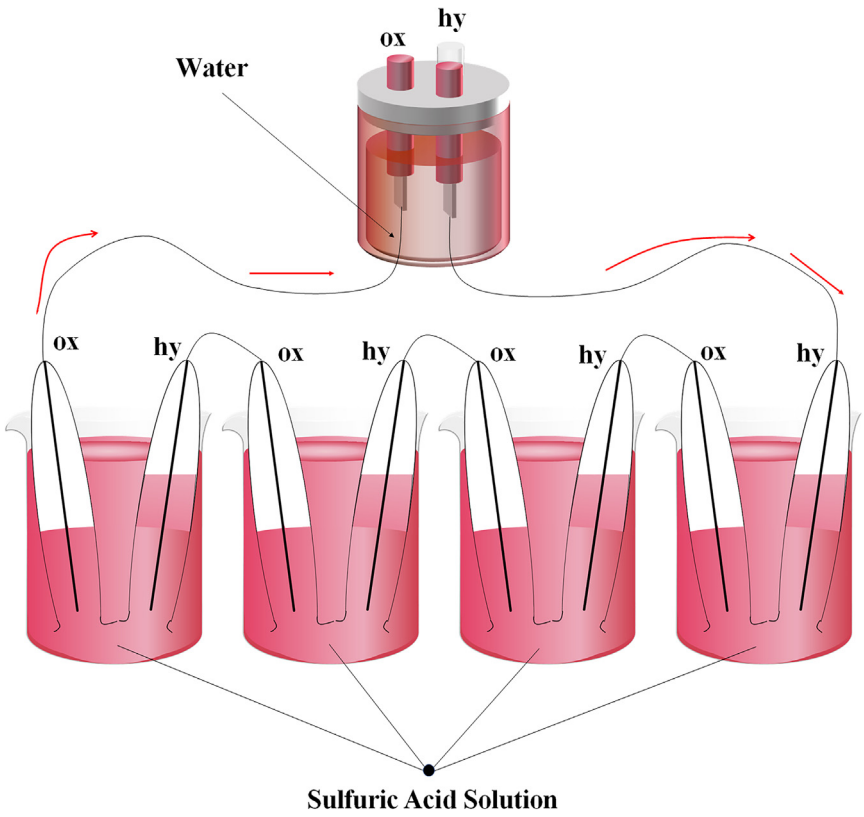

Figure 1. Sketch of William Grove's 1839 fuel cell

Grove's 1839 gas voltaic battery diagram. (From *Proceedings of the Royal Society*) [1] Redrawn with permission of Taylor & Francis Journal.

More radical approaches may be necessary to challenge the 300–600°C operational range. Here we review novel functional nanocomposites that show a high promise for that range. The focus will be on ceria-based and multifunctional semiconductor-ionic electrolytes.

CERIA-BASED COMPOSITES AND NANOCOMPOSITES AS ALTERNATIVE ELECTROLYTE MATERIALS

Cation-doped cerium oxide, especially samarium doped ceria (SDC) and gadolinium doped ceria (GDC) have a fluoride structure, extensively studied as O^{2-} conducting electrolyte in SOFC.[19] However, there are some crucial problems with doped ceria. Firstly, to reach a high 0.1 S/cm oxygen ion conductivity, a temperature of 800°C is still required. At 600°C, doped ceria show only 10^{-3} – 10^{-2} S/cm.[20,21] Secondly, Ce^{4+} in ceria may reduce to Ce^{3+} in the reducing fuel cell leading to significant electronic conduction, causing electrochemical and a lower open-circuit voltage (OCV).[22] Also, the considerable size difference between Ce^{4+} (87p.m.) and Ce^{3+} (102p.m.) may cause some micro-cracking in the fuel cell operations leading to device failure.[23]

To solve these problems, improved ceria-based composites and nanocomposites have been developed, e.g., ceria-carbonate composites, successfully demonstrated at 300–600°C in low-temperature (LT) SOFC.[24–37] In ceria-carbonate composites, the ionic conductivity is enhanced by the composite melting effects, where the molten carbonate provides a solid-liquid interface resulting in high ionic transport. The interfacial regions between the two phases cause a combined effect, i.e., each constituent phase has high ionic conduction. Fabricating two- or multi-phase composites thus produces more interface regions, i.e., a kind of ionic conduction highway. Various ceria-salt composites (e.g., metal chlorites, metal hydrates, carbonates, and sulfates) have been investigated, where ceria-carbonate, such as samarium doped ceria (SDC), gadolinium doped ceria (GDC), yttrium doped ceria (YDC), Ca/Sm-co-doped CeO_2 (CSDC), etc., composites have been combined with various metal carbonates, $MxCO_3$ (M+ Li, Na, K, Ca, Ba, Sr, x = 1, 2) in single, Na, binary, Li-Na, Li-K, Na-K and ternary Li-Na-K, etc. systems [8–45].[31,38–63] These ceria-carbonate

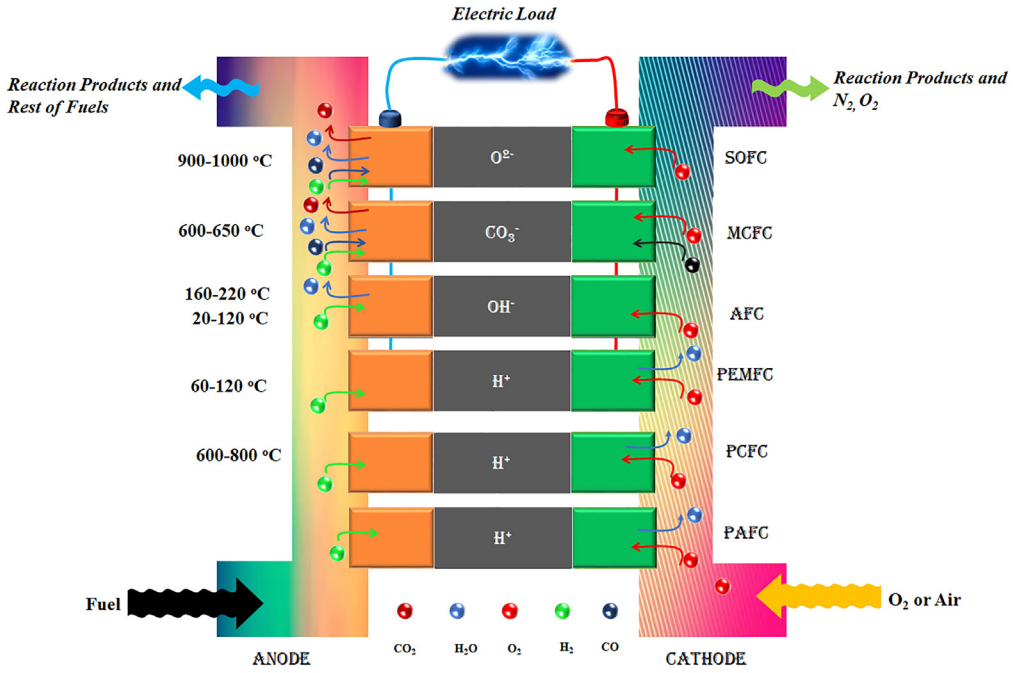

Figure 2. Classification of fuel cells by the electrolyte

composite systems have been used as electrolytes to demonstrate successful LT-SOFC operation. Ceria-carbonate composites have also shown excellent thermal and electrochemical stability,[28,59,60] even standing long 6000-h tests.[61]

Most of these ceria-composites have not employed nanocomposite methodologies to make more controllable material microstructures and properties to improve the reproducibility and stability of the electrolyte.

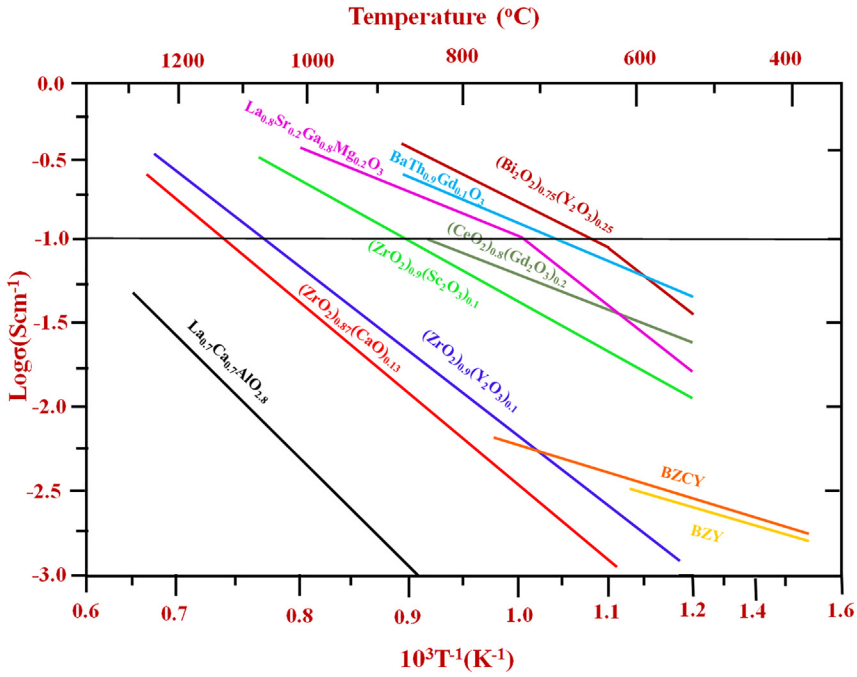

Figure 3. Oxide-ion conductor candidates for SOFCs and PCFCs.[15]
Modified from[15] with permission Elsevier.

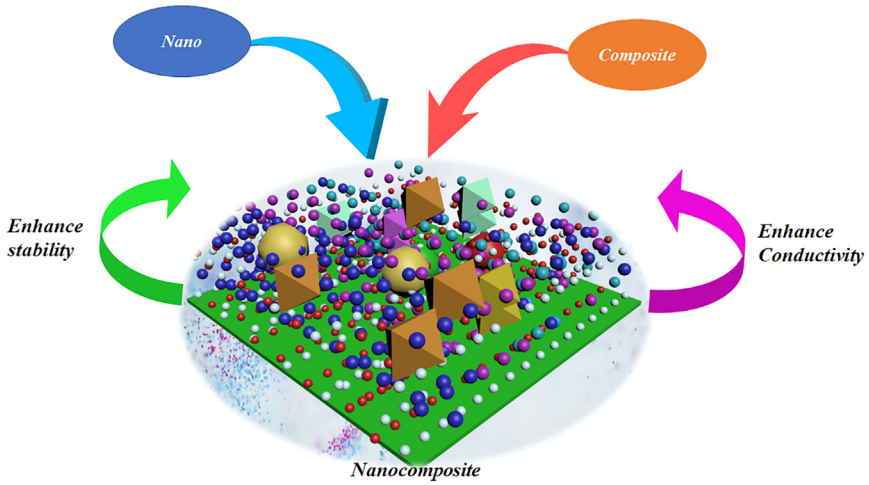

Figure 4. Illustration of the nanocomposite approach

Nano effects have enhanced material grain boundary or surface ionic conduction, particularly in ceria and zirconia-based materials.[64] However, at high temperatures (600–800°C), nano effects may be lost, and in ceria-based materials, the nano-effects may also increase the electronic conduction. It has been proposed to introduce a second-phase material to build up a heterostructure that could effectively block nanoparticle growth and significantly enhance ionic conductivity by modulating interfacial structures.[63]

The principal differences between the ceria-carbonate composites and nanocomposites are in the morphology shown in Figure 4 and the material properties and functionality. Figures 5A–5D shows that standard ceria-carbonate composites are irregular sharps of two-phase particles. Most of them reach a percolative mixture threshold in which two phases can form percolative paths along interface regions to maintain the combined effect, i.e., ionic conduction through the interfaces between the two-phase areas of the materials. This can only be possible when the carbonate melts. Figure 5F shows an intensive endothermic peak at about 497°C in the DTA curves, related to the melting of 53 mol%Li_2CO_3:47 mol%Na_2CO_3 carbonate eutectic. The conductivity leap occurs at the carbonate melting point to the molten phase in Figure 5E.[33,57,64]

The particles are homogeneous for the nanocomposite, e.g., SDC-Na_2CO_3, as shown in Figure 6A. In the HRTEM images in Figure 6B, there is a clear core-shell structure with very thin (a few nm) shells of sodium carbonate covering the SDC nanoparticles. The composite can still form continuous interfacial regions to build fast ionic conducting channels along the SDC particle surfaces or two phases of SDC and Na_2CO_3 interfaces. The nanocomposite approach has successfully been employed to develop novel functional ceria-based nanocomposite materials, e.g., core-shell samarium doped ceria (SDC)-sodium carbonate.[64,65] The most crucial difference between ceria-carbonate composites and nanocomposites relates to the carbonate maintaining its physical property. Reaching the carbonate melting point leading to high ionic conductivity requires at least a 20% carbonate share, which also causes corrosion with molten carbonates.[65] Binary or trinary complex carbonate systems could be used to maintain the stability of ceria-carbonate composite electrolytes for use in LT-SOFC at temperatures below 600°C. In the SDC-Na_2CO_3 core-shell nanocomposite, the Na_2CO_3 does not keep its property. There is a phase transition already at around 300°C, much lower than the Na_2CO_3 melting point (851°C).[40] In this case, the nanocomposite well maintains a solid phase property avoiding the molten carbonate corrosion problem. More importantly, the ceria-carbonate nanocomposite exhibits novel properties in the solid mechanical phase and superionic conduction, which is more advanced than in a regular ceria-carbonate composite.[65] Figure 6D shows that a superionic transition occurs in the Na_2CO_3@SDC nanocomposite so that the ionic conductivity is well above 0.1 S/cm in the temperature range of 300–550°C. In the DSC thermal analysis, an endothermic peak is found in Figure 6E indicates a microstructure ordering change because the material's two phases are maintained and melting does not occur.[39]

The novel core-shell amorphous SDC/Na_2CO_3 nanocomposite in Figure 6B has a particle size of less than 100 nm. The thickness of the amorphous Na_2CO_3 shell is 4–6 nm forming a solid type of nanocomposite that displays high ionic conductivity over 0.1 S/cm above 300°C. Amorphous Na_2CO_3 and core-shell

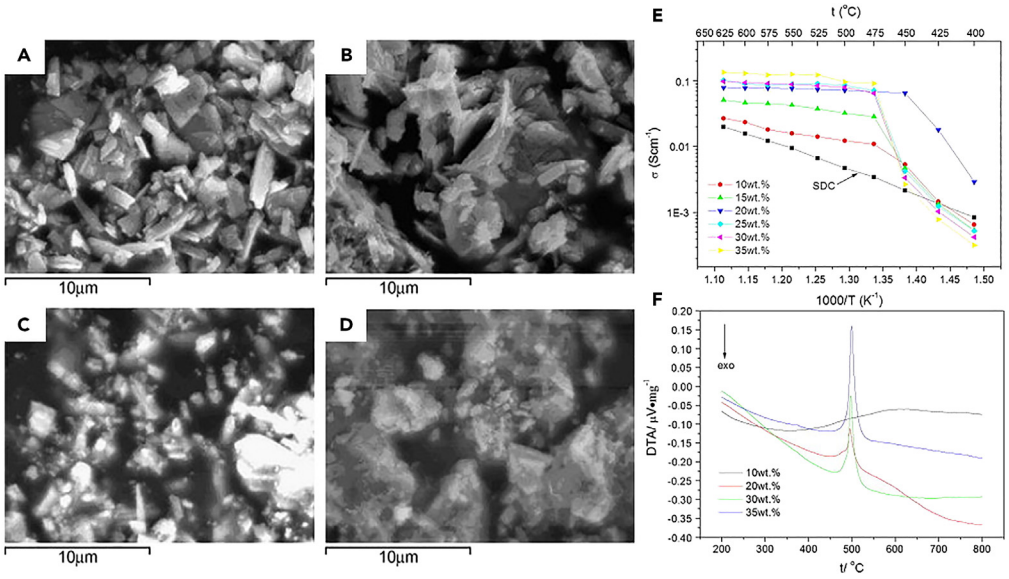

Figure 5. Ceria carbonate composites and electrical properties of SDC/NCO

SEM images of SDC-(53 mol% Li_2CO_3: 47 mol% Na_2CO_3) composites with carbonate content of (A) 10 wt %, (B) 20 wt %, (C) 30 wt %, and (D) 35 wt %,[64] (E) conductivities' of composites with various carbonate contenet based on temperature dependence; (F) correspondingly, the DTA curves for SDC-(53 mol% Li_2CO_3:47 mol% Na_2CO_3) composites with various carbonate contents conductivities' temperature dependence[64] with permission of Elsevier.

structure may play an essential role in the ionic conductivity attributed to the interface and interfacial conduction mechanism. In addition, Fan et al. have presented the practical synthesis of element/phase well-distributed, interfacial strongly linked $Sm_{0.2}Ce_{0.8}O_2$-Na_2CO_3 (NSDC) nanocomposite with varied residual carbonate contents by an *in situ* one-pot one-step citric acid-nitrate combustion process. NSDC has increased ionic conductivity over conventionally prepared materials. NSDC9010 nanocomposite proton conductivity is 0.044 S/cm at 650°C. Electrolyte-supported SOFCs based on NSDC9010 nanocomposite electrolyte produce 281.5 mW cm^2 at 600°C with $LiNiO_2$ symmetric electro-catalysts. The unique core-shell structure, good phase distribution, and high interfacial area created by the one-step fabrication approach and the strong coupling between oxide and carbonate contribute to the superior ionic

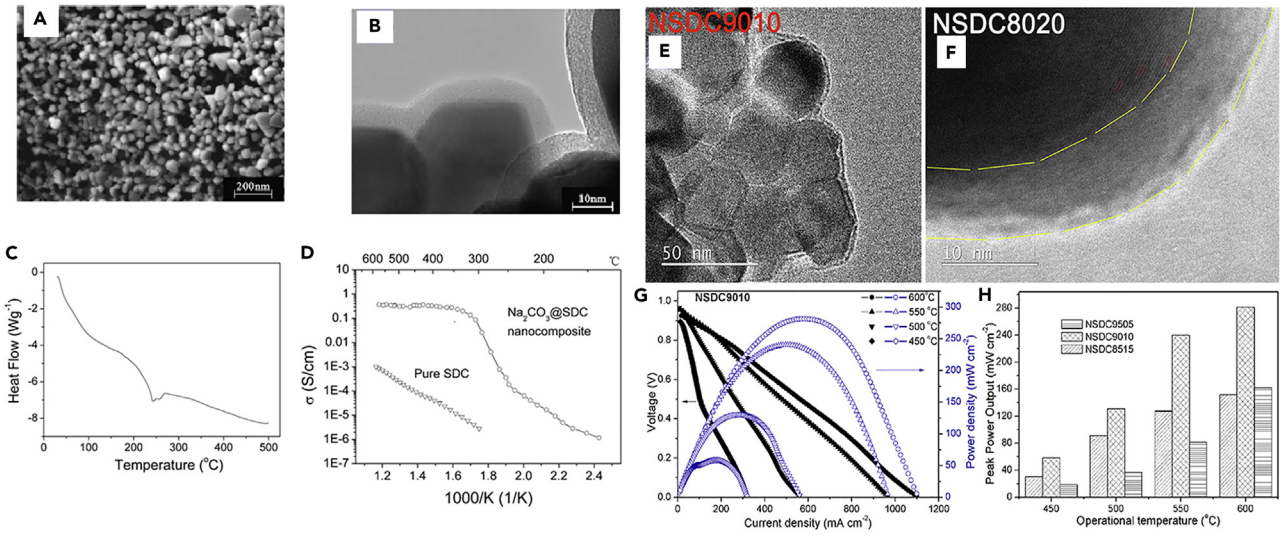

Figure 6. Morphology, electrical and electrochemical properties of nanocomposites

(A) SEM image, (B) HRTEM image, (C) DSC curve, and (D) dependence of the conductivity vs. temperature of as-prepared SDC/Na_2CO_3 nanocomposite, (E–H) HR-TEM images and fuel cell performance and comparison of NSDC Copyright[65,66] with permission of elsewhere.

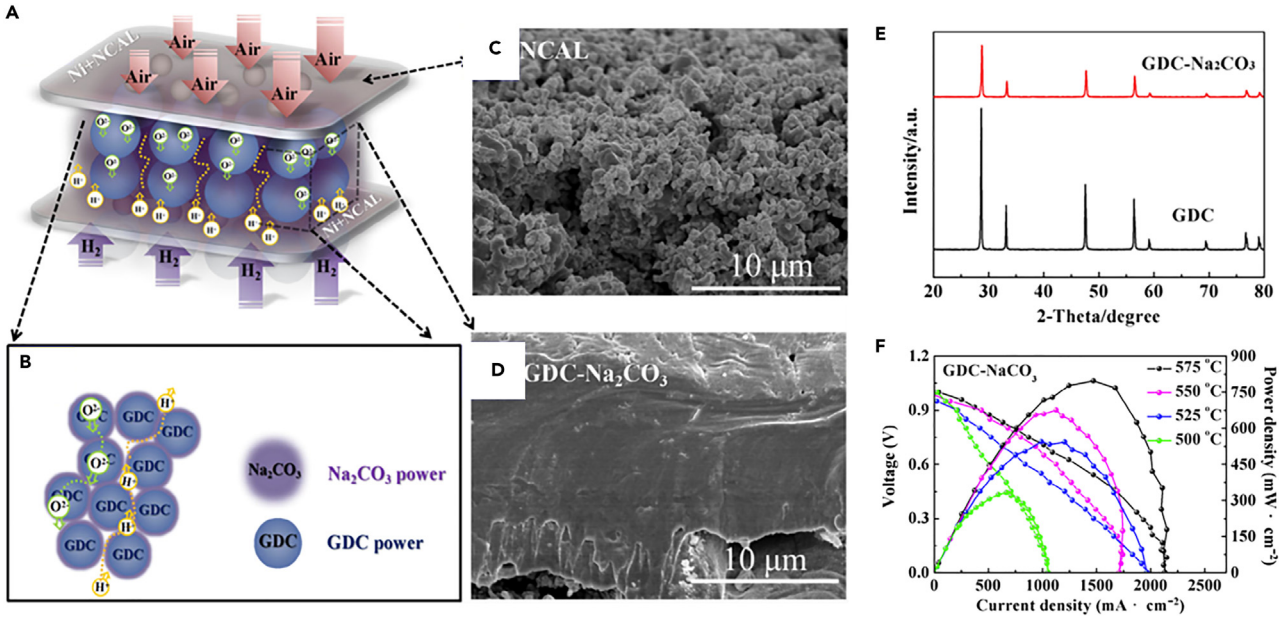

Figure 7. Conduction path for protons and ions along with morphology, stuctural and electrochemical properties of GDC/NCO

(A and B) Schematic diagram of fuel cell device with GDC-Na_2CO_3 electrolyte and NCAL electrode along with the conduction path of protons and oxide ions, (C and D) SEM image of NCAL porous electrode and electrolyte membrane GDC-Na_2CO_3, (E and F) XRD analysis of GDC, GDC-Na_2CO_3, and performance of GDC-Na_2CO_3 electrolyte membrane[67] with permission of John Wiley and Sons.

conductivity and fuel cell performance.[66] The HR-TEM images of NSDC and fuel cell performance of NSDC9010 and comparison of fuel cell performance between the NSDC9010 and NSDC9505, NSDC8515 are shown in Figures 6E–6H. The ceria-carbonate in composite (molten-solid) or nanocomposite (solid-solid) interface may present a new approach to designing and developing superionic conductors for low-temperature SOFCs. Creating a 'superionic highway' interface in two-phase materials based on the coated ceria-carbonate composites has demonstrated a new way to realize SOFC/PCFC at 300–600°C.

Figure 7A illustrates a structural schematic diagram of the GDC-Na_2CO_3 fuel cell.[67] Symmetrical electrodes $Ni_{0.8}Co_{0.15}Al_{0.05}LiO_{2-\delta}$ (NCAL) were used for redox functionality, whereas GDC-Na_2CO_3 works as an electrolyte to conduct the ions. Figure 7B shows the conduction path of protons and oxide ions through the electrolyte to accomplish the fuel cell reactions. Furthermore, the morphology of NCAL reveals the fluffy and well-porous structure assists in mass transfer with the extension of the triple-phase boundary depicted in Figure 7C. At the same time, GDC-Na_2CO_3 seems too dense without pores after sintering at 575 C, and the desired density assists in separating the H_2 and air gases or prevents the contact between air and H_2, as illustrated in Figure 7D. The XRD of GDC and GDC-Na_2CO_3 reveal a pure fluorite structure. Still, with the addition of Na_2CO_3, the peak intensity is lower, and slight expansion is noticed, confirming the formation of a GDC-Na_2CO_3 structure without impurity peaks, as demonstrated in Figure 7E.[22,67] During the fuel cell operation, it is known that Na_2CO_3 changes into a molten state and makes connections or bonds with other materials, as seen in the examples with SDC-Na_2CO_3, GDC-Na_2CO_3, etc., to attain nanocomposite material characteristics.[67] The relationship between the functions of the different particles as quick ions transport channels simultaneously speeds up the process leading to enhanced electrochemical fuel cell performance with a power density of 800 mW/cm^2 at 575 C shown in Figure 7F. Moreover, several studies have been reported to enhance the ionic conduction and boost the fuel cell performance using the above stated phenomena.[37,45,62,67–69]

Recently it has been reported that pure ceria (CeO_2) has shown fast ion transportation through surface conduction which is different from the traditional concept of doping ceria.[70] Xing et al. designed a non-stoichiometry $CeO_{2-\delta}$ forming CeO_2@$CeO_{2-\delta}$ core-shell structure to build up a fast proton shuttle on the surface layer, as shown in Figures 8A and 8B. It exhibited excellent proton conductivity at 0.16 S/cm and 697 mW/cm^2 at 520°C as depicted in Figures 8C and 8D.[71]

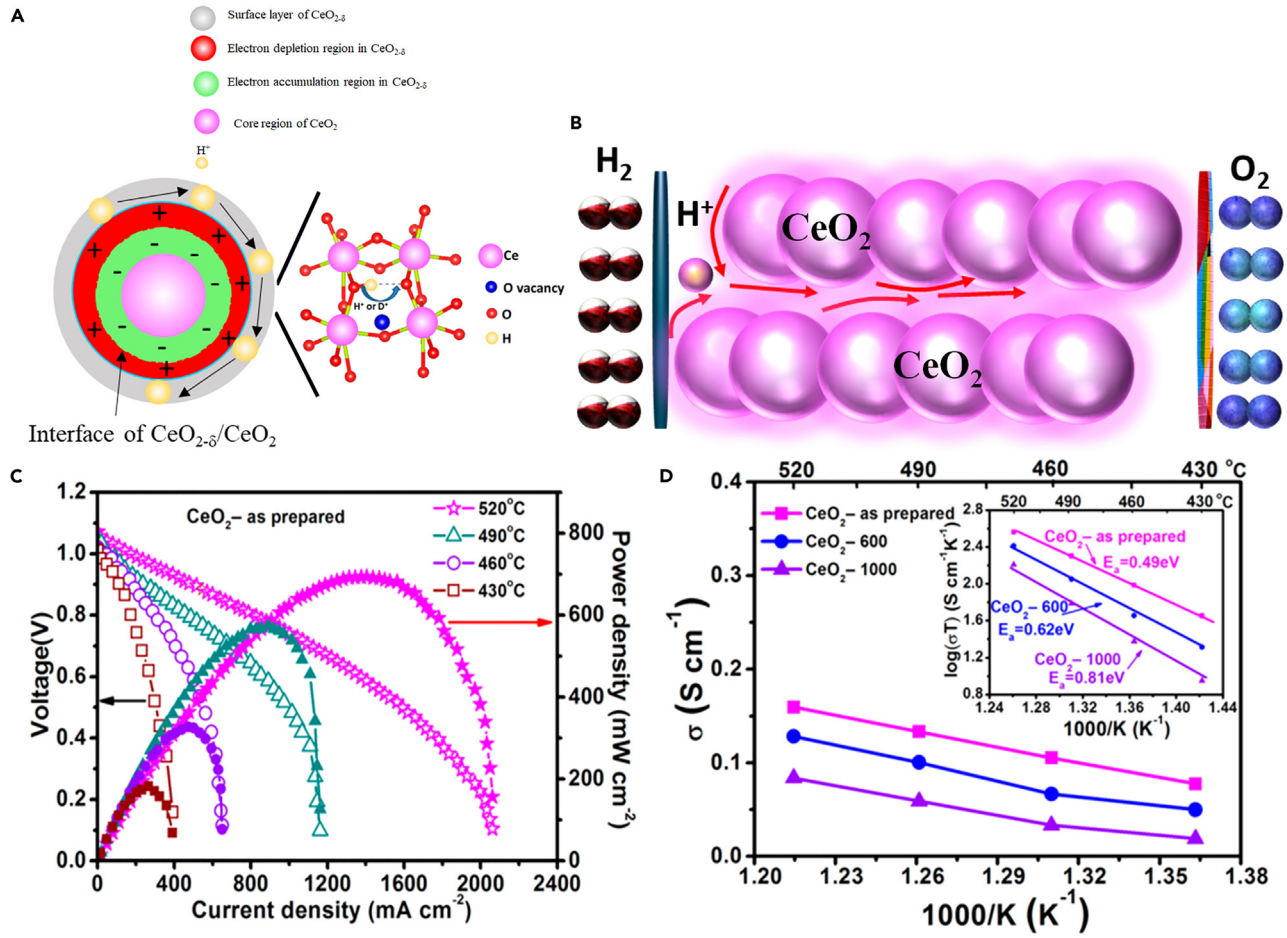

Figure 8. Proton shuttle mechnism and electrical & electrochemical properties of non-doped ceria

(A–D) Non-doping CeO_2 with a non-stichometry $CeO_{2-\delta}$ shell forming the core-shell structure resulting in high performance and fast proton conduction taken from[71] permission with ACS.

Xia et al. synthesized non-doped CeO_2 through the co-precipitation technique using different precipitating agents (Na_2CO_3, NH_4HCO_3, and KOH). The best performance was achieved using Na_2CO_3 as a precipitating agent, suggesting that Na_2CO_3 is a powerful agent in building strong bondage and long-lasting channels for quick ion transportation and enhancing the device performance.[72] The designed fuel cell device based on the CeO_2-Na_2CO_3 delivered 706 mW/cm^2 at 550°C.[72] The high performance is because of the morphological effect confirmed in the HAADAF-STEM image and cross-bonding mapping of each element, including Na, Ce, and O, as depicted in Figures 9A and 9B. Furthermore, one CeO_2 particle was selected for morphology analysis, where it seems to be covered with an amorphous layer of Na_2CO_3 shown in Figures 9C and 9D. The TEM images confirm that the CeO_2 is covered with a thin coating layer of Na_2CO_3 where the thickness of the coating layer was 3 nm with a lattice spacing of 0.19 nm related to the 220 planes of CeO_2 as depicted in Figures 9E and 9F. Figure 9G shows the schematic diagram of the fuel cell based on the CeO_2 electrolyte and the CeO_2 particles covered with a thin layer to function as a core-shell structure that also prevents the CeO_2 from reducing, which is a major issue with pure CeO_2.[70,71,73] Fan et al. use a self-doping approach to prepare a core-shell nanocomposite of CeO_2 and alkali carbonates (Li_2CO_3, Na_2CO_3, and K_2CO_3) At 550°C in air, a remarkable ionic conductivity of 0.34 S/cm was formed, unlike the insulating CeO_2 phase. The single-cell electrochemical performance reached 910 mW/cm^2.[74] All the above literature shows that the carbonates and the combined effect with doped and non-doped CeO_2 are very favorable in enhancing the device performance. The high ionic conductivity achieved also paves the way to develop a new electrolyte for SOFC/PCFC at lower temperatures than the traditional ones.

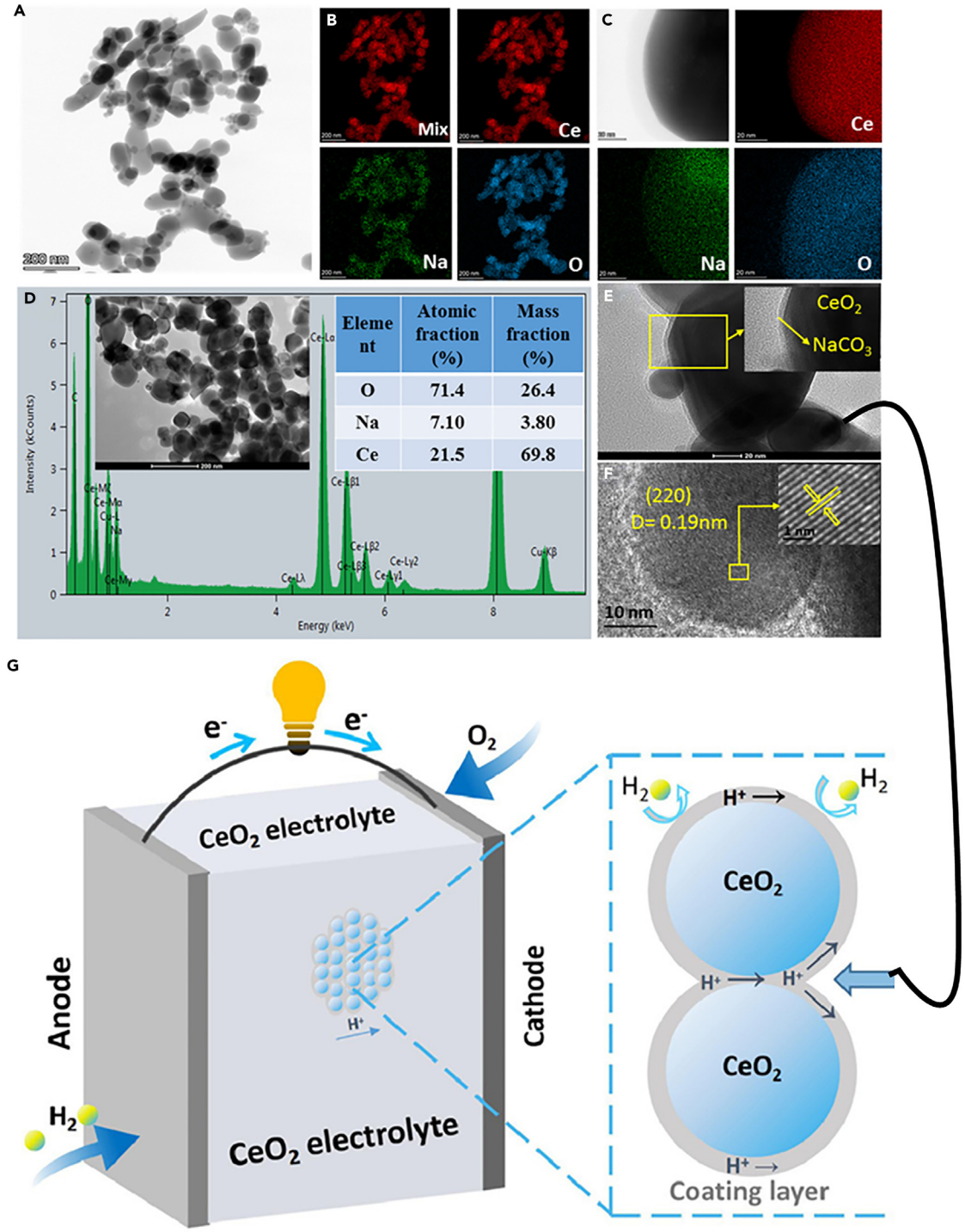

Figure 9. Morophology and mechnism of ions transport using surface layer in non-doped Ceria

(A and B) HAADAF-STEM image and elemental mapping of CeO_2-Na_2CO_3 particles (C and D) HAADAF-STEM and elemental mapping along with elemental composition atomic fraction and mass fraction of CeO_2-Na_2CO_3, (E–G) HR-TEM images of CeO_2-Na_2CO_3 and Fuel cell diagram with a zoomed-in view of CeO_2 particle coated with Na_2CO_3 layer[72] with permission of Elsevier.

Besides the electrolyte ionic conduction, the redox process is equally crucial for constructing the composite electrolyte and electrodes. Ceria-based electrolytes have been frequently used as a catalyst because of their excellent redox properties originating from the reduction of Ce^{+4} to Ce^{+3} oxidation state.[31] Two

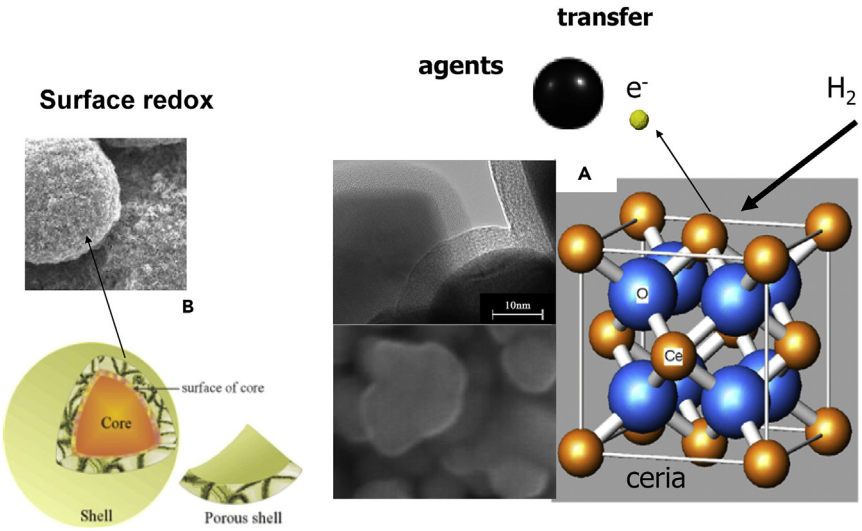

Figure 10. Redox design of composite electrolyte

Redox design by using second-phase materials acting as an agent for electron acceptor and donor for composite electrolyte (A) and electrode (B)[31] with permission of Elsevier.

oxides with good redox properties have often been combined: For example, $MCeO_2$, where M could be Gd, Sm, Ca, Mn, Pr, Y, and many more, plus M_xO_y structure in which M could be Bi, Co, Ti, Ni, and V whereas x and y can be in the range of 1–3 and 1–4, respectively.[31]

In the Ce-structure, incorporating the second phase, such as an electron acceptor phase, efficiently receives electrons to work as a redox agent. The two-phase composite material can turn into an efficient pure ionic conducting electrolyte material in comparison to pure CeO_2, as depicted in Figure 10. The exact mechanism is probably applicable to construct composite electrodes, which can be accomplished using several nano-redox catalyst particles such as NiO distributed and coated with ceria shown in Figures 10A and 10B.[31,75–78] Table 1 shows different composite electrolytes using ceria-based composites and their performance at different temperatures.

MULTIFUNCTIONAL SEMICONDUCTOR-IONIC NANOCOMPOSITES

To illustrate the concept of multifunctional electrolyte materials, Figure 11 shows a metal oxide semiconductor (MOS) of LiZnOx (or ½ Li2O–ZnO) with an ionic material SDC.[82,84] Figure 11A displays the HRTEM image of LiZnOx-SDC nanocomposite where the nano-SDC particle as a core covered by a thin layer of LiZnOx.

ZnO is an n-type semiconductor and can react with Li_2O to form ½ Li_2O–ZnO or a LiZnOx compound. In LiZnOx-SDC semiconductor nanocomposite, the LiZnOx is coated on the SDC nanoparticles (less than 100 nm), forming a two-phase core-shell heterostructure (see HRTEM, Figures 11A and 11B). This particular core-shell microstructure can significantly enhance ionic conductivity reaching >0.1 S cm^{-1} at ca. 300°C, which is equivalent to pure SDC at 800°C or YSZ at 1000°C, as depicted in Figure 11C. A conventional single-phase structure cannot achieve such an enhancement—the ionic conductivity benefits here, particularly from interfacial effects.

Another type of semiconductor-ionic heterostructure is found in the yttria-stabilized zirconia (YSZ)/strontium titanate $SrTiO_3$ (STO)-YSZ thin-film composite system.[85] The YSZ is a typical ionic conductor used in the traditional SOFC. STO is a standard semiconductor, which, together with YSZ, thus forms a semiconductor-ionic system. This system has shown several orders of magnitude higher ionic conductivity enhancement than the pure YSZ.[85] The heterostructures where YSZ layers in the nanometer range (i-62 nm) and were fabricated between two 10 nm thick $SrTiO_3$ (STO) layers. Figure 12 shows the electrical properties of the 1 nm-YSZ layer.

Table 1. Ceria-based composite electrolyte materials for fuel cells

Nr	Ceria-carbonates	Gases	Conductivity (S/cm)	Power density (W/cm^2)	Operating temperature (°C)	Reference
[1]	GDC-salt composites	H_2/Air	0.01–1	0.20–0.8	400–660	Zhu et al.[79]
[2]	YDC-22 wt % $LiNaCO_3$	H_2/Air	0.01–0.78	0.20–0.70	400–660	Zhu et al.[79]
[3]	GYDC-40 wt % $LiKCO_3$	H_2/Air	–	0.07–0.30	480–530	Zhu et al.[79]
[4]	SDC-10 wt % $LiNaCO_3$	H_2/Air	0.001–0.03	0.43	400–625	Huang et al.[64]
[5]	SDC-20 wt % $LiNaCO_3$	H_2/Air	0.003–0.09	0.94	400–625	Huang et al.[64]
[6]	SDC-30 wt % $LiNaCO_3$	H_2/Air	0.003–0.1	0.89	400–625	Huang et al.[64]
[7]	SDC-35 wt % $LiNaCO_3$	H_2/Air	0.1–0.15	1.08	400–625	Huang et al.[64]
[8]	SDC-30 wt % $LiNaCO_3$	H_2/Air	0.01–0.2	0.2–1.0	500–650	Huang et al.[80]
[9]	SDC-30 wt % $LiNaKCO_3$	H_2/Air	0.05–0.2	0.1–0.76	500–700	Xia et al.[58]
[10]	SDC-30 wt % $LiNaCO_3$	H_2/(CO_2/O_2)	0.05–0.16	0.3–1.70	500–650	Xia et al.[58]
[11]	GDC-30 wt % $LiKCO_3$	H_2/Air	0.002–0.09	–	300–700	Benamira et al.[81]
[12]	CeO_2-nanocomposite	H_2/Air	–	0.20–0.70	450–580	Raza et al.[82]
[13]	SDC-Na_2CO_3 nanocomposite	H_2/Air	–	0.50–0.90	450–580	Wang et al.[65]
[14]	GYDC-$LiNaCO_3$	H_2/Air	0.2	0.6	550	Zhang et al.[83]

The STO-YSZ epitaxial heterostructure system can show up to eight orders of magnitude enhancement near room temperature.[85] Enhancing the ionic conductivity and a YSZ layer thickness–independent conductivity implies an interface process. This may be because of the atomic reconstruction at the interface between highly different structures between the fluorite YSZ and perovskite STO, yielding colossal ionic conductivity values, where the interfaces play a significant role in enhancing the ionic conductivity massively. The coherent interface between very different structures can also significantly decrease the activation energy, thus greatly improving ionic mobility and increasing conductivity.[85] This result is of paramount technological importance to achieving high O^{2-} conduction at low temperatures.

The STO-YSZ system may have three parallel conduction paths from the interfaces and the bulk YSZ and STO layers. However, the bulk conductivity of YSZ is only 10^{-7} S/cm at 500°C. On the other hand, the reported conductivity values of the STO thin films are also much lower than those obtained with high conductance. Therefore, bulk YSZ or STO contributions can be ruled out, and an interface conduction mechanism is suggested instead. In addition, there is an abrupt conductivity decrease when the thickness changes from 30 to 62 nm. This may indicate a loss of interface structure when the YSZ layers exceed the critical

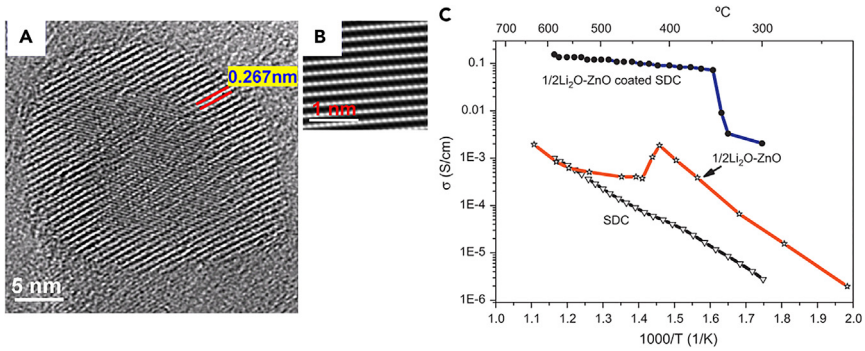

Figure 11. Morphology and electrical feature of SDC/LZO

(A) A high-resolution TEM image showing a core-shell structure of an SDC nanoparticle covered by a thin layer of LiZnOx;
(B) simulated HRTEM image of ZnO coating at [2 1 0] projection.
(C) The dependence of the conductivity of non-coated SDC and LiZn-oxide coated SDC on the temperature in comparison with the conductivity curve of 1/2Li_2O–ZnO cited from literature reported by Tsukamoto et al.[84] with permission Elsevier.

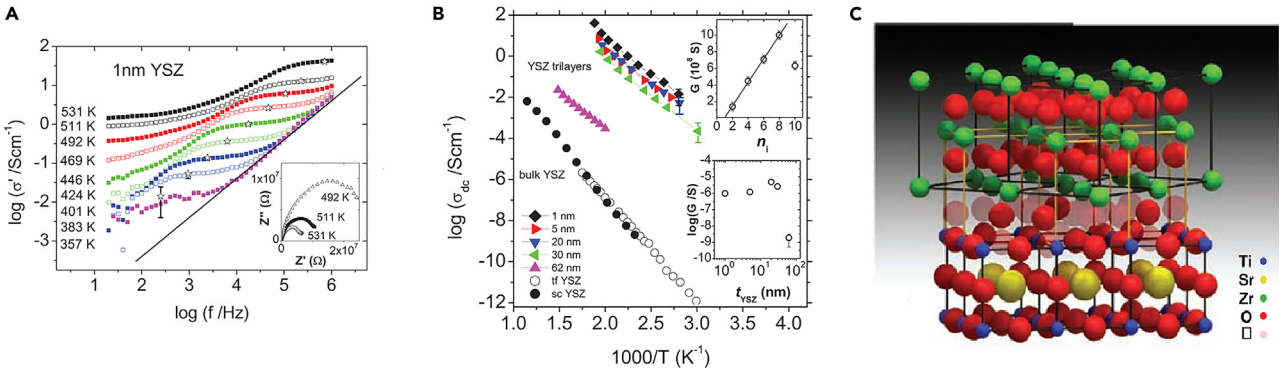

Figure 12. The electrical properties of YSZ/STO and 3D view of the interface of YSZ/STO

(A) The real part of the lateral electrical conductivity versus frequency of the tri-layer with 1-nm thick YSZ in the 357 to 531 K range. The uncertainty of conductance measurements is 1 n-S (10^{-2} S/cm in conductivity for the sample shown, see error bar)(Inset) Imaginary versus real part of the impedance (Nyquist) plots at 492, 511, and 531 K.

(B) Dependence of the ionic conductivity of the trilayers STO/YSZ/STO versus inverse temperature. The thickness range of the YSZ layer is 1–62 nm. (Top inset) 400 K conductance of [YSZ1nm/STO10 nm] (ni/2) superlattices as a function of the number of interfaces. (Bottom inset) Dependence of the conductance of [STO10nm/YSZ Xnm/STO10nm] trilayers at 500 K on YSZ layer thickness. Error bars are according to a 1 nS uncertainty of the conductance measurement.

(C) A 3D view of the interface, with the ionic radius reduced by half, to better visualize the plane of oxygen vacancies introduced in the interface. The square symbol in the legend indicates the empty positions available for oxygen ions at interface.[85] Copyright permission from Science.

thickness that the bulk behavior turns to effect.[85] Further improvement of microstructural characterization (effective interfacial area and percolative pathways), explaining the interfacial conditions, and effective ionic transport and charge transfer under different working conditions are still required to understand the fundamental aspects better.

As shown in Figure 13, semiconductor-ionic material (SIM) systems have been widely investigated for various structural materials such as fluorite, perovskite, spinel, and layered structure systems.[9,67,70,85–108] These heterostructure composite systems based on ionic-MOS or semiconductor-semiconductor materials make use of interfaces and interactions in the interfacial regions between two constituent phases, which result in interfacial conduction and charge transport highways, with significant impacts on the superionic conduction, redox reactions (hydrogen oxidation and oxygen reduction), catalyst, electrolysis, and fuel cell. The material architecture of the two-phase composite demonstrates a new scientific principle of material design and development, where the surface and interfacial mechanisms cause the conductivity and charge transfer enhancement.

For example, Zhu et al. designed a semiconductor (LSCF), $La_{0.6}Sr_{0.4}Co_{0.2}Fe_{0.8}O_{3-\delta}$ ionic (SCDC) Sm/Ca-co-doped Ceria electrolyte owing specific properties toward a new generation of fuel cells. The utilized SIM electrolyte has revealed high ionic and electronic conductivity of >0.1 S/cm, higher OCV (>1.0 V), and fuel cell performance of 1000 mW/cm^2 at 550°C. The HR-TEM image of the semiconductor ionic (LSCF-SCDC) heterostructure is shown in Figure 14B, whereas the energy band alignment mechanism is depicted in Figure 14C.[109] In the same context, Xia and Mushtaq have designed new semiconductor ionic electrolyte materials, including STO-SDC ($SrTiO_3$-$Sm_{0.2}Ce_{0.8}O_2$), SFT-SDC ($SrFe_{0.75}Ti_{0.25}O_{3-\delta}$-$Sm_{0.25}Ce_{0.75}O_2$) and delivered impressive fuel cell performance of 892 and 920 mW/cm^2 with higher ionic conductivity of 0.14 and >0.1 S/cm at a low operating temperature of 550 and 520°C respectively.[110,111] The Energy band diagram of SFT-SDC and schematic diagram including ORR and HOR mechanism, fuel cell performance, and SEM cross-sectional view of the pellet have been depicted in Figures 14A, 14D, and 14E. Furthermore, new semiconductor ionic heterostructure CeO_2/BZY was used as an electrolyte, revealing maximum proton conduction of 0.23 S/cm and impressive fuel cell performance of 845 mW/cm^2 at 520°C. Figures 14F and 14G shows the energy band diagram and proton transport mechanism on the surface and interface of CeO_2& BZY.[112] In addition, a new semiconductor heterostructure ($LiCoO_2$-SnO_2) based on bulk, bulk planar, and the thin-film-based planar junction was proposed as an electrolyte. It displayed higher fuel cell performance of 0.82, 0.61, and 0.28 W/cm^2 at 600°C. Figure 14H shows the schematic diagram of a fuel cell of bulk heterostructure $LiCoO_2$-SnO_2 with fuel cell performance of different ratios between the LCO and SnO_2 at a constant operational temperature of 600°C.[113] The above-stated mechanism and

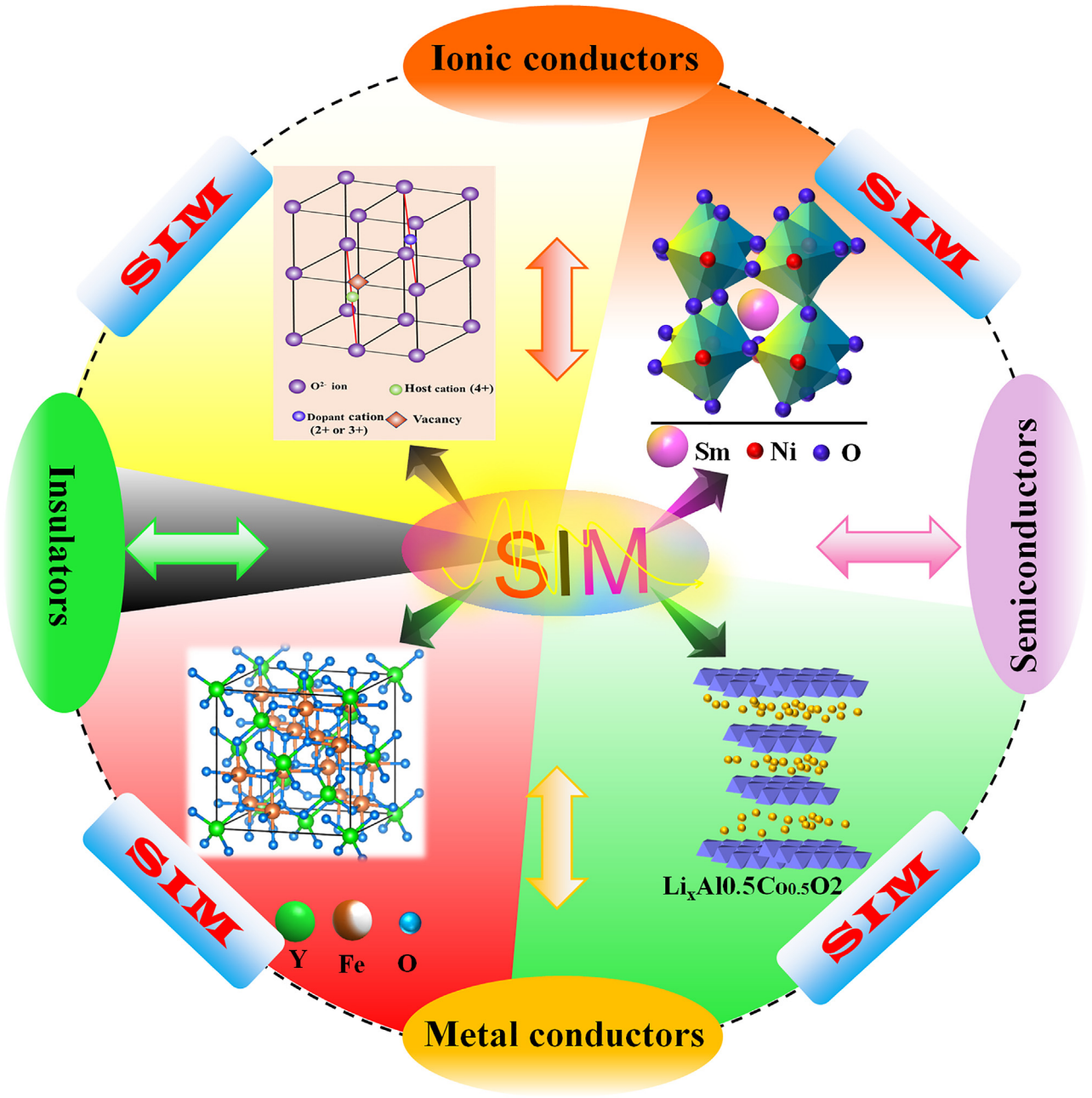

Figure 13. Semiconductor-ionic material (SIM) systems

Semiconductor-ionic material (SIM) systems with various structural materials such as fluorite, perovskite, spinel, and layered structure systems.

reports differ from the conventional single-phase materials such as YSZ and SDC/GDC etc., where the high conductivity is realized by aliovalent doping to create oxygen vacancies inside the structure (a bulk mechanism), and device gaps/interfaces between the different components, e.g., anode, electrolyte, and cathode, which requires complex technology and strict condition to make the device functions, e.g., high temperature are needed to activate ionic mobility.[9]

CONCLUDING REMARKS

The electrolyte materials have been the focus of developing SOFC technologies since Nernst first discovered the YSZ with a fluoride structure, as shown in Figure 15. Figure 15A shows that a low valency cation

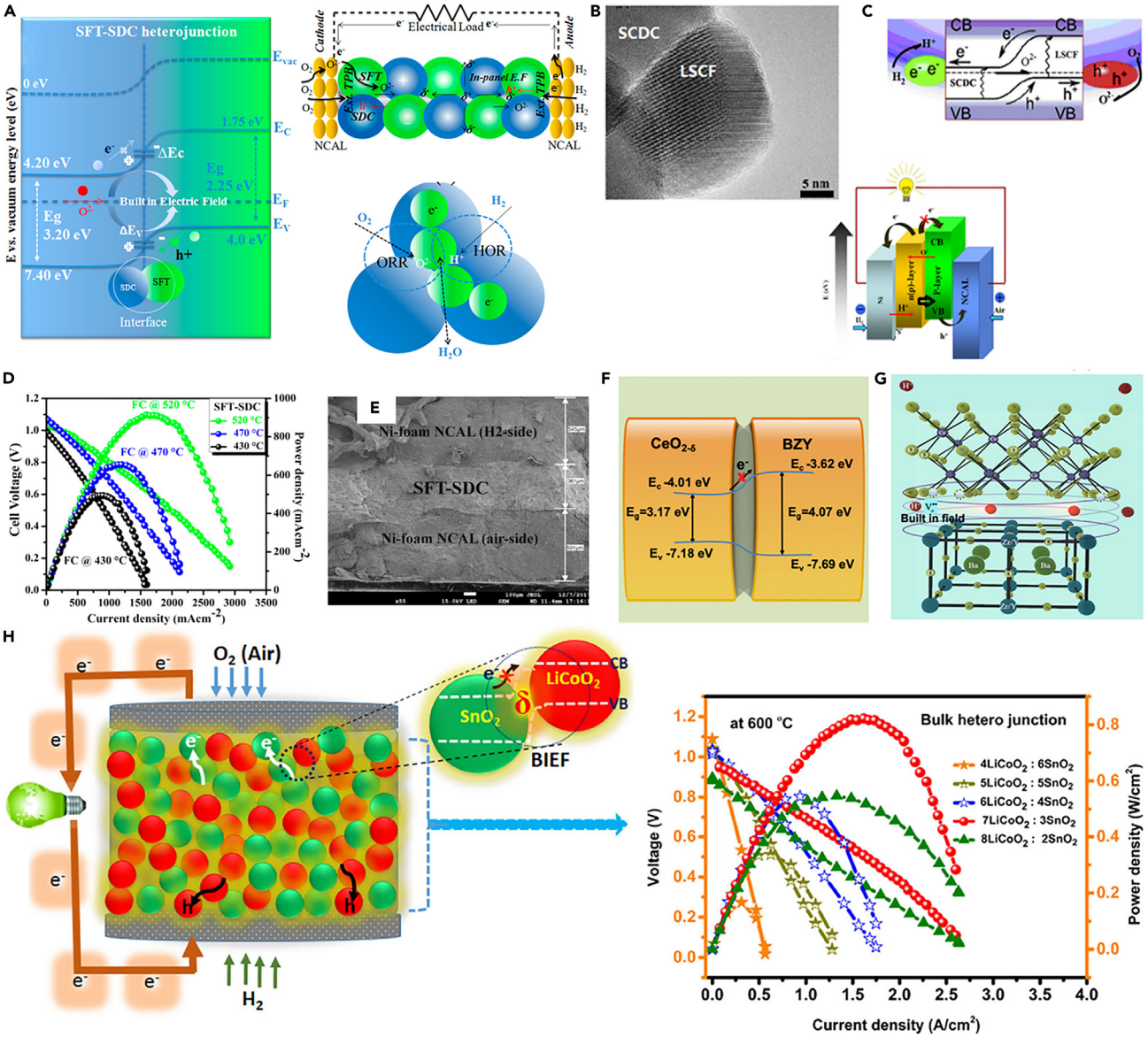

Figure 14. Energy band alingment, conduction mechnism and fuel cell performance of SFT-SDC, LSCF-SCDC, BZY/CeO_2 and LCO/SnO_2

(A) Energy band diagram of SFT-SDC and schematic diagram with HOR and ORR mechanism, (B and C) HR-TEM image of LSCF/SCDC and Energy band alignment mechanism, (D and E) I-V/I-P curve and SEM cross-sectional view of SFT-SDC, (F and G) Energy band diagram and proton transport mechanism on the surface of CeO_2/BZY, (H) Schematic diagram based on bulk heterostructure $LiCoO_2$-SnO_2 with fuel cell performance of composite heterostructures.[109,111–113] Copyright permission from the American Chemical Society and Elsevier.

dopant, e.g., rare earth ions of Y^{3+} or $Sm^{3+,}$ to replace high valency Zr^{4+} or Ce^{4+} to create oxygen vacancy, enables the oxygen ion O^{2-} to move through this vacancy. This structural design methodology has been central for the SOFC electrolyte and proton-conducting perovskites (BZ & BZY), as shown in Figures 15B and 15C.[9,114] Replacing YSZ with new materials with high ionic conductivity at reduced temperatures, e.g., below 600°C, has not been successful so far.[9,20]

The novel ceria-based nanocomposites and semiconductor-ionic heterostructure material systems reviewed in this paper represent new radical developments that could pave the way to next-generation low-temperature ceramic fuel cells operating in the range of 300–600°C at high power density. The underlying reason for such a performance improvement is surficial and interfacial ionic conduction.[115] These materials rely on different design methodologies and functionalities than the traditional SOFC changing from

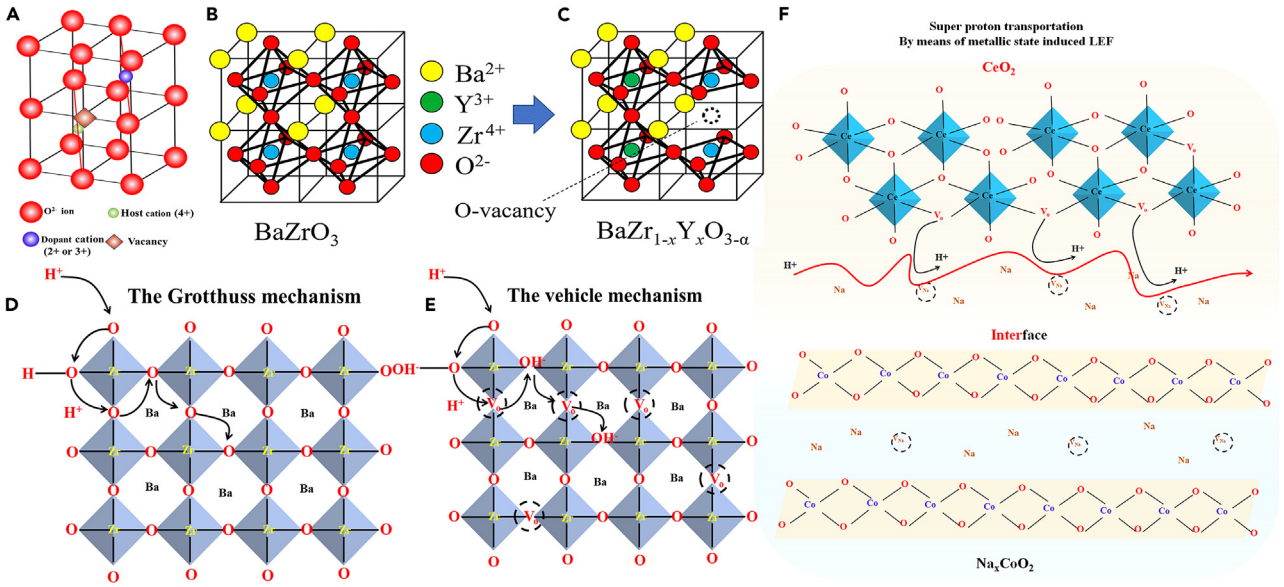

Figure 15. Ionic conduction from structure design to semiconductor heterostructure

(A) O^{2-} conducting fluoride with low valency cation dopant replace high valency Zr^{4+} or Ce^{4+} to create oxygen vacancy, then O^{2-} move through this vacancy; perovskite proton conductor by the same way doping to create oxygen vacancies in (B) BaZrO3 structure to form (C) BZYO; and protons can move with two mechanisms as illustrated in (D) Grotthuss lattice oxygen transfer and (E) oxygen vacancy-vehicle mechanism. (F) in strong contrast, the superionic conduction is designed based on semiconductor heterostructure, e.g., $pNaCoO_3$-$nCeO_2$, where interfacial conduction mechanism with the help of built-in-electric field as a self-driving force on ionic transport[9,18,114,115] permission with Elsevier, and Science.

the bulk inside the structure to particle surface and interfaces (Figures 15D–15F), especially the semiconductor heterostructure.

More interestingly, from these novel functional semiconductor heterostructure composite systems, the ionic conducting electrolyte concept can now be expanded on electrolyte-free or semiconductor membrane fuel cells based on the nano-redox principle,[93,116,117] where a built-in-electric field can act as the second driving force to promote ionic transport.[116,117] The fundamental understanding of this semiconductor-based membrane fuel cell technology is developed into a new discipline of semiconductor electrochemistry,[98] which deserves more attention for next-generation fuel cell technology. We have reviewed novel solid material systems with high potential for next-generation fuel cells at 300–600°C. These employ ceramic nanocomposites based on semiconductor-ionic materials, either with core-shell or heterojunction structures. Power densities up to 1 Wcm^{-2} could be reached with these materials when used in a fuel cell device.

ACKNOWLEDGMENTS

This work was supported by Southeast University (SEU) project 3203002003A1 and National Natural Science Foundation of China (NSFC) under the grant 51772080 and 11604088. Jiangsu Provincial Innovation and Entrepreneurship Talent program Project No. JSSCRC2021491. Industry-University-Research Cooperation Project of Jiangsu Province in China, Grant No. BY2021057.

AUTHOR CONTRIBUTIONS

M.A.K.Y.S.: Writing – original draft, redrawing figures, review and editing; B.Z. and P.D.L.: Revision, writing, editing, and supervision.

DECLARATION OF INTERESTS

The author declares no competing interests.

REFERENCES

1. Grove, W.R. (1839). XXIV. On voltaic series and the combination of gases by platinum. London, Edinburgh Dublin Phil. Mag. J. Sci. *14*, 127–130.
2. Steele, B.C., and Heinzel, A. (2011). Materials for fuel-cell technologies. In Materials for sustainable energy: a collection of peer-reviewed research and review articles from Nature Publishing Group (World Scientific), pp. 224–231.
3. Wilson, J.R., Kobsiriphat, W., Mendoza, R., Chen, H.-Y., Hiller, J.M., Miller, D.J., Thornton, K., Voorhees, P.W., Adler, S.B., and Barnett, S.A. (2006). Three-dimensional reconstruction of a solid-oxide fuel-cell anode. Nat. Mater. *5*, 541–544.
4. Haile, S.M., Boysen, D.A., Chisholm, C.R., and Merle, R.B. (2001). Solid acids as fuel cell electrolytes. Nature *410*, 910–913.
5. Jacobson, M.Z., Colella, W.G., and Golden, D.M. (2005). Cleaning the air and improving health with hydrogen fuel-cell vehicles. Science *308*, 1901–1905.
6. Jacobson, A.J. (2010). Materials for solid oxide fuel cells. Chem. Mater. *22*, 660–674.
7. Kerman, K., Lai, B.K., and Ramanathan, S. (2012). Nanoscale compositionally graded thin-film electrolyte membranes for low-temperature solid oxide fuel cells. Adv. Energy Mater. *2*, 656–661.
8. Chen, Y.-Y., and Wei, W.-C.J. (2006). Processing and characterization of ultra-thin yttria-stabilized zirconia (YSZ) electrolytic films for SOFC. Solid State Ionics *177*, 351–357.
9. Goodenough, J.B. (2000). Oxide-ion conductors by design. Nature *404*, 821–823.
10. Singhal, S. (2013). The SOFC-XIII Satellite Seminar, *10*, SOFC Market and Commercialization: Overview, Okinawa.
11. Saebea, D., Authayanun, S., Patcharavorachot, Y., Chatrattanawet, N., and Arpornwichanop, A. (2018). Electrochemical performance assessment of low-temperature solid oxide fuel cell with YSZ-based and SDC-based electrolytes. Int. J. Hydrogen Energy *43*, 921–931.
12. Naiqing, Z., Kening, S., Derui, Z., and Dechang, J. (2006). Study on properties of LSGM electrolyte made by tape casting method and applications in SOFC. J. Rare Earths *24*, 90–92.
13. Bi, L., Da'as, E.H., and Shafi, S.P. (2017). Proton-conducting solid oxide fuel cell (SOFC) with Y-doped BaZrO3 electrolyte. Electrochem. Commun. *80*, 20–23.
14. Yang, L., Zuo, C., and Liu, M. (2010). High-performance anode-supported Solid Oxide Fuel Cells based on Ba (Zr0. 1Ce0. 7Y0. 2) O3− δ (BZCY) fabricated by a modified co-pressing process. J. Power Sources *195*, 1845–1848.
15. Singhal, S.C., and Kendall, K. (2003). High-temperature Solid Oxide Fuel Cells: Fundamentals, Design and Applications (Elsevier).
16. Iwahara, H., Uchida, H., Ono, K., and Ogaki, K. (1988). Proton conduction in sintered oxides based on BaCeO3. J. Electrochem. Soc. *135*, 529–533.
17. Iwahara, H., Esaka, T., Uchida, H., and Maeda, N. (1981). Proton conduction in sintered oxides and its application to steam electrolysis for hydrogen production. Solid State Ionics *3–4*, 359–363.
18. Hossain, M.K., Hashizume, K., and Hatano, Y. (2020). Evaluation of the hydrogen solubility and diffusivity in proton-conducting oxides by converting the PSL values of a tritium imaging plate. Nucl. Mater. Energy *25*, 100875.
19. Park, H.C., and Virkar, A.V. (2009). Bimetallic (Ni–Fe) anode-supported solid oxide fuel cells with gadolinia-doped ceria electrolyte. J. Power Sources *186*, 133–137.
20. Steele, B. (2000). Appraisal of Ce Gd O electrolytes for IT-SOFC operation at 12y y 22y/2 5008C. Solid State Ionics *129*, 95–110.
21. Wachsman, E.D., and Lee, K.T. (2011). Lowering the temperature of solid oxide fuel cells. Science *334*, 935–939.
22. Jamale, A.P., Bhosale, C.H., and Jadhav, L.D. (2016). Fabrication and characterization of La0.6Sr0. 4Co0.2Fe0. 8O3-δ (LSCF)-Ce0.9Gd0. 1O1. 95 (GDC) composite thick film for anode supported solid oxide fuel cells. J. Mater. Sci. Mater. Electron. *27*, 795–799.
23. Li, Y.T., Xie, M.K., Wu, J., and Wang, S. (2014). Chemical stability study of nanoscale thin film yttria-doped barium cerate electrolyte for micro solid oxide fuel cells. Biomed. Rep. *2*, 804–808.
24. Zhu, B. (2001). Advantages of intermediate temperature solid oxide fuel cells for tractionary applications. J. Power Sources *93*, 82–86.
25. Zhu, B., Liu, X., Zhou, P., Yang, X., Zhu, Z., and Zhu, W. (2001). Innovative solid carbonate–ceria composite electrolyte fuel cells. Electrochem. Commun. *3*, 566–571.
26. Zhu, B., Yang, X., Xu, J., Zhu, Z., Ji, S., Sun, M., and Sun, J. (2003). Innovative low temperature SOFCs and advanced materials. J. Power Sources *118*, 47–53.
27. Ferreira, A.S., Soares, C.M., Figueiredo, F.M., and Marques, F.M. (2011). Intrinsic and extrinsic compositional effects in ceria/carbonate composite electrolytes for fuel cells. Int. J. Hydrogen Energy *36*, 3704–3711.
28. Li, X., Xiao, G., and Huang, K. (2011). Effective ionic conductivity of a novel intermediate-temperature mixed oxide-ion and carbonate-ion conductor. J. Electrochem. Soc. *158*, B225.
29. Ma, Y., Wang, X., Li, S., Toprak, M.S., Zhu, B., and Muhammed, M. (2010). Samarium-doped ceria nanowires: novel synthesis and application in low-temperature solid oxide fuel cells. Adv. Mater. *22*, 1640–1644.
30. Amar, I.A., Lan, R., Petit, C.T., Arrighi, V., and Tao, S. (2011). Electrochemical synthesis of ammonia based on a carbonate-oxide composite electrolyte. Solid State Ionics *182*, 133–138.
31. Raza, R., Zhu, B., Rafique, A., Naqvi, M.R., and Lund, P. (2020). Functional ceria-based nanocomposites for advanced low-temperature (300–600° C) solid oxide fuel cell: a comprehensive review. Mater. Today Energy *15*, 100373.
32. Gao, Z., Huang, J., Mao, Z., Wang, C., and Liu, Z. (2010). Preparation and characterization of nanocrystalline Ce0.8Sm0. 2O1. 9 for low temperature solid oxide fuel cells based on composite electrolyte. Int. J. Hydrogen Energy *35*, 731–737.
33. Huang, J., Gao, R., Mao, Z., and Feng, J. (2010). Investigation of La2NiO4+ δ-based cathodes for SDC–carbonate composite electrolyte intermediate temperature fuel cells. Int. J. Hydrogen Energy *35*, 2657–2662.
34. Jia, L., Tian, Y., Liu, Q., Xia, C., Yu, J., Wang, Z., Zhao, Y., and Li, Y. (2010). A direct carbon fuel cell with (molten carbonate)/(doped ceria) composite electrolyte. J. Power Sources *195*, 5581–5586.
35. Zhao, Y., Xia, C., Wang, Y., Xu, Z., and Li, Y. (2012). Quantifying multi-ionic conduction through doped ceria-carbonate composite electrolyte by a current-interruption technique and product analysis. Int. J. Hydrogen Energy *37*, 8556–8561.
36. Dong, X., Tian, L., Li, J., Zhao, Y., Tian, Y., and Li, Y. (2014). Single layer fuel cell based on a composite of Ce0. 8Sm0. 2O2− δ–Na2CO3 and a mixed ionic and electronic conductor Sr2Fe1. 5Mo0. 5O6− δ. J. Power Sources *249*, 270–276.
37. Zhao, Y., Xu, Z., Xia, C., and Li, Y. (2013). Oxide ion and proton conduction in doped ceria–carbonate composite materials. Int. J. Hydrogen Energy *38*, 1553–1559.
38. Fang, J., Li, M., Li, Q., Zhang, W., Shou, Q., Liu, F., Zhang, X., and Cheng, J. (2012). Microwave-assisted synthesis of CoAl-layered double hydroxide/graphene oxide composite and its application in supercapacitors. Electrochim. Acta *85*, 248–255.
39. Zhao, L., Huang, X., Zhu, R., Lu, Z., Sun, W., Zhang, Y., Ge, X., Liu, Z., and Su, W. (2008). Optimization on technical parameters for fabrication of SDC film by screen-printing used as electrolyte in IT-SOFC. J. Phys. Chem. Solid. *69*, 2019–2024.
40. Ma, Y., Wang, X., Raza, R., Muhammed, M., and Zhu, B. (2010). Thermal stability study of SDC/Na2CO3 nanocomposite electrolyte

for low-temperature SOFCs. Int. J. Hydrogen Energy *35*, 2580–2585.

41. Li, X., Xu, N., Zhang, L., and Huang, K. (2011). Combining proton conductor BaZr0. 8Y0. 2O3-δ with carbonate: promoted densification and enhanced proton conductivity. Electrochem. Commun. *13*, 694–697.

42. Di, J., Chen, M., Wang, C., Zheng, J., Fan, L., and Zhu, B. (2010). Samarium doped ceria–(Li/Na) 2CO3 composite electrolyte and its electrochemical properties in low temperature solid oxide fuel cell. J. Power Sources *195*, 4695–4699.

43. Qin, H., Zhu, Z., Liu, Q., Jing, Y., Raza, R., Imran, S., Singh, M., Abbas, G., and Zhu, B. (2011). Direct biofuel low-temperature solid oxide fuel cells. Energy Environ. Sci. *4*, 1273–1276.

44. Liu, Q., and Zhu, B. (2010). Theoretical description of superionic conductivities in samaria doped ceria based nanocomposites. Appl. Phys. Lett. *97*, 183115.

45. Wang, X., Ma, Y., Li, S., Kashyout, A.-H., Zhu, B., and Muhammed, M. (2011). Ceria-based nanocomposite with simultaneous proton and oxygen ion conductivity for low-temperature solid oxide fuel cells. J. Power Sources *196*, 2754–2758.

46. Zhang, L., Lan, R., Kraft, A., and Tao, S. (2011). A stable intermediate temperature fuel cell based on doped-ceria–carbonate composite electrolyte and perovskite cathode. Electrochem. Commun. *13*, 582–585.

47. Mizuhata, M., Ohashi, T., and Béléké, A.B. (2010). Electrical conductivity of the coexisting system containing molten carbonates and rare-earth oxide. ECS Trans. *33*, 439–447.

48. Fan, L., Wang, C., Chen, M., and Zhu, B. (2013). Recent development of ceria-based (nano) composite materials for low temperature ceramic fuel cells and electrolyte-free fuel cells. J. Power Sources *234*, 154–174.

49. Raza, R., Ahmad, M.A., Iqbal, J., Akram, N., Gao, Z., Javed, S., and Zhu, B. (2014). Ce0. 8 (SmZr) 0.2 O2-carbonate nanocomposite electrolyte for solid oxide fuel cell. Int. J. Energy Res. *38*, 524–529.

50. Khan, M.A., Raza, R., Lima, R.B., Chaudhry, M.A., Ahmed, E., Khalid, N., Abbas, G., Zhu, B., and Nasir, N. (2014). Effect of titania concentration on the grain boundary conductivity of calcium-doped ceria electrolyte. Ceram. Int. *40*, 9775–9781.

51. Zhu, B., Lund, P., Raza, R., Patakangas, J., Huang, Q.-A., Fan, L., and Singh, M. (2013). A new energy conversion technology based on nano-redox and nano-device processes. Nano Energy *2*, 1179–1185.

52. Zhu, B., Lund, P.D., Raza, R., Ma, Y., Fan, L., Afzal, M., Patakangas, J., He, Y., Zhao, Y., Tan, W., et al. (2015). Schottky junction effect on high performance fuel cells based on nanocomposite materials. Adv. Energy Mater. *5*, 1401895.

53. Fan, L., Zhu, B., Chen, M., Wang, C., Raza, R., Qin, H., Wang, X., Wang, X., and Ma, Y. (2012). High performance transition metal oxide composite cathode for low temperature solid oxide fuel cells. J. Power Sources *203*, 65–71.

54. Abbas, G., Chaudhry, M.A., Raza, R., Singh, M., Liu, Q., Qin, H., and Zhu, B. (2012). Study of CuNiZnGdCe-nanocomposite anode for low temperature SOFC. Nanosci. Nanotechnol. Lett. *4*, 389–393.

55. Hu, J., Tosto, S., Guo, Z., and Wang, Y. (2006). Dual-phase electrolytes for advanced fuel cells. J. Power Sources *154*, 106–114.

56. Zhu, B. (2006). Next generation fuel cell R&D. Int. J. Energy Res. *30*, 895–903.

57. Huang, J., Xie, F., Wang, C., and Mao, Z. (2012). Development of solid oxide fuel cell materials for intermediate-to-low temperature operation. Int. J. Hydrogen Energy *37*, 877–883.

58. Xia, C., Li, Y., Tian, Y., Liu, Q., Zhao, Y., Jia, L., and Li, Y. (2009). A high performance composite ionic conducting electrolyte for intermediate temperature fuel cell and evidence for ternary ionic conduction. J. Power Sources *188*, 156–162.

59. Li, Y., Rui, Z., Xia, C., Anderson, M., and Lin, Y. (2009). Performance of ionic-conducting ceramic/carbonate composite material as solid oxide fuel cell electrolyte and CO2 permeation membrane. Catal. Today *148*, 303–309.

60. Rui, Z., Anderson, M., Lin, Y., and Li, Y. (2009). Modeling and analysis of carbon dioxide permeation through ceramic-carbonate dual-phase membranes. J. Membr. Sci. *345*, 110–118.

61. Bodén, A., Di, J., Lagergren, C., Lindbergh, G., and Wang, C.Y. (2007). Conductivity of SDC and (Li/Na) 2CO3 composite electrolytes in reducing and oxidising atmospheres. J. Power Sources *172*, 520–529.

62. Wang, X., Ma, Y., and Zhu, B. (2012). State of the art ceria-carbonate composites (3C) electrolyte for advanced low temperature ceramic fuel cells (LTCFCs). Int. J. Hydrogen Energy *37*, 19417–19425.

63. Fan, L., Zhu, B., Su, P.-C., and He, C. (2018). Nanomaterials and technologies for low temperature solid oxide fuel cells: recent advances, challenges and opportunities. Nano Energy *45*, 148–176.

64. Huang, J., Mao, Z., Liu, Z., and Wang, C. (2007). Development of novel low-temperature SOFCs with co-ionic conducting SDC-carbonate composite electrolytes. Electrochem. Commun. *9*, 2601–2605.

65. Wang, X., Ma, Y., Raza, R., Muhammed, M., and Zhu, B. (2008). Novel core–shell SDC/amorphous Na2CO3 nanocomposite electrolyte for low-temperature SOFCs. Electrochem. Commun. *10*, 1617–1620.

66. Zhang, G., Deng, X., Guan, F., Bai, Z., Cao, L., Mao, H., Tang, C., Li, C., He, C., and Zhang, Q. (2018). Strongly coupled Sm0. 2Ce0. 8O2-Na2CO3 nanocomposite for low temperature solid oxide fuel cells: one-step synthesis and super interfacial proton conduction. Clin. Biomech. *57*, 56–66.

67. Zhou, X., Xia, C., Wang, X., Dong, W., and Wang, B. (2020). Improving grain boundary conductivity of Ce0.9Gd0. 1O2−δ electrolyte through compositing with carbonate or semiconductor. Energy Technol. *8*, 2000424.

68. Yue Bai, J., Wang, L., Jing Wang, H., Fei Huang, P., Qing Zhao, Y., and Di Fan, S. (2006). Electrochemical behavior and determination of epinephrine at a mercaptoacetic acid self-assembled gold electrode. Microchim. Acta *156*, 321–326.

69. Huang, J., Yang, L., Gao, R., Mao, Z., and Wang, C. (2006). A high-performance ceramic fuel cell with samarium doped ceria–carbonate composite electrolyte at low temperatures. Electrochem. Commun. *8*, 785–789.

70. Wang, B., Zhu, B., Yun, S., Zhang, W., Xia, C., Afzal, M., Cai, Y., Liu, Y., Wang, Y., and Wang, H. (2019). Fast ionic conduction in semiconductor CeO2-δ electrolyte fuel cells. NPG Asia Mater. *11*, 51.

71. Xing, Y., Wu, Y., Li, L., Shi, Q., Shi, J., Yun, S., Akbar, M., Wang, B., Kim, J.-S., and Zhu, B. (2019). Proton shuttles in CeO2/CeO2−δ core–shell structure. ACS Energy Lett. *4*, 2601–2607.

72. Akbar, M., Jin, B., Tu, Z., Gao, J., Yousaf, M., Mushtaq, N., Wang, X., Dong, W., Wang, B., Cai, Y., and Xia, C. (2021). High-performing and stable non-doped ceria electrolyte with amorphous carbonate coating layer for low-temperature solid oxide fuel cells. Electrochim. Acta *393*, 139067.

73. Kim, J.-T., Lee, T.-H., Park, K.-Y., Seo, Y., Kim, K.B., Song, S.-J., Park, B., and Park, J.-Y. (2015). Electrochemical properties of dual phase neodymium-doped ceria alkali carbonate composite electrolytes in intermediate temperature. J. Power Sources *275*, 563–572.

74. Jing, Y., Lund, P., Asghar, M.I., Li, F., Zhu, B., Wang, B., Zhou, X., Chen, C., and Fan, L. (2020). Non-doped CeO2-carbonate nanocomposite electrolyte for low temperature solid oxide fuel cells. Ceram. Int. *46*, 29290–29296.

75. Chen, Y., Lin, Y., Zhang, Y., Wang, S., Su, D., Yang, Z., Han, M., and Chen, F. (2014). Low temperature solid oxide fuel cells with hierarchically porous cathode nano-network. Nano Energy *8*, 25–33.

76. Zhang, C. (2016). Solid oxide fuel cells: low temperature cathodes. Nat. Energy *1*, 16200–16202.

77. Li, P., Zhao, Y., Yu, B., Li, J., and Li, Y. (2015). Improve electrical conductivity of reduced

La2Ni0. 9Fe0. 1O4+ δ as the anode of a solid oxide fuel cell by carbon deposition. Int. J. Hydrogen Energy *40*, 9783–9789.

78. Peng, X., Tian, Y., Liu, Y., Wang, W., Pu, J., Li, J., Chi, B., and Li, J. (2020). A double perovskite decorated carbon-tolerant redox electrode for symmetrical SOFC. Int. J. Hydrogen Energy *45*, 14461–14469.

79. Zhu, B. (2003). Functional ceria–salt-composite materials for advanced ITSOFC applications. J. Power Sources *114*, 1–9.

80. Huang, J., Mao, Z., Liu, Z., and Wang, C. (2008). Performance of fuel cells with proton-conducting ceria-based composite electrolyte and nickel-based electrodes. J. Power Sources *175*, 238–243.

81. Benamira, M., Ringuedé, A., Albin, V., Vannier, R.-N., Hildebrandt, L., Lagergren, C., and Cassir, M. (2011). Gadolinia-doped ceria mixed with alkali carbonates for solid oxide fuel cell applications: I. A thermal, structural and morphological insight. J. Power Sources *196*, 5546–5554.

82. Raza, R., Abbas, G., Wang, X., Ma, Y., and Zhu, B. (2011). Electrochemical study of the composite electrolyte based on samaria-doped ceria and containing yttria as a second phase. Solid State Ionics *188*, 58–63.

83. Zhang, L., Lan, R., Petit, C.T., and Tao, S. (2010). Durability study of an intermediate temperature fuel cell based on an oxide–carbonate composite electrolyte. Int. J. Hydrogen Energy *35*, 6934–6940.

84. Wu, J., Zhu, B., Mi, Y., Shih, S.-J., Wei, J., and Huang, Y. (2012). A novel core–shell nanocomposite electrolyte for low temperature fuel cells. J. Power Sources *201*, 164–168.

85. Garcia-Barriocanal, J., Rivera-Calzada, A., Varela, M., Sefrioui, Z., Iborra, E., Leon, C., Pennycook, S.J., and Santamaria, J. (2008). Colossal ionic conductivity at interfaces of epitaxial ZrO2: Y2O3/SrTiO3 heterostructures. Science *321*, 676–680.

86. Zhou, Y., Guan, X., Zhou, H., Ramadoss, K., Adam, S., Liu, H., Lee, S., Shi, J., Tsuchiya, M., Fong, D.D., and Ramanathan, S. (2016). Strongly correlated perovskite fuel cells. Nature *534*, 231–234.

87. Chen, G., Zhu, B., Deng, H., Luo, Y., Sun, W., Liu, H., Zhang, W., Wang, X., Qian, Y., Hu, X., et al. (2018). Advanced fuel cell based on perovskite La–SrTiO3 semiconductor as the electrolyte with superoxide-ion conduction. ACS Appl. Mater. Interfaces *10*, 33179–33186.

88. Shah, M.Y., Mushtaq, N., Rauf, S., Akbar, N., Xing, Y., Wu, Y., Wang, B., and Zhu, B. (2020). Advanced fuel cell based on semiconductor perovskite La–BaZrYO3-δ as an electrolyte material operating at low temperature 550° C. Int. J. Hydrogen Energy *45*, 27501–27509.

89. Singh, K., Nowotny, J., and Thangadurai, V. (2013). Amphoteric oxide semiconductors for energy conversion devices: a tutorial review. Chem. Soc. Rev. *42*, 1961–1972.

90. Shah, M.A.K.Y., Zhu, B., Rauf, S., Mushtaq, N., Yousaf, M., Ali, N., Tayyab, Z., Akbar, N., Yang, C.P., and Wang, B. (2020). Electrochemical properties of a co-doped SrSnO3− δ-based semiconductor as an electrolyte for solid oxide fuel cells. ACS Appl. Energy Mater. *3*, 6323–6333.

91. Hu, E., Jiang, Z., Fan, L., Singh, M., Wang, F., Raza, R., Sajid, M., Wang, J., Kim, J.-S., and Zhu, B. (2021). Junction and energy band on novel semiconductor-based fuel cells. iScience *24*, 102191.

92. Rauf, S., Zhu, B., Shah, M., Tayyab, Z., Attique, S., Ali, N., Mushtaq, N., Asghar, M., Lund, P., and Yang, C. (2021). Low-temperature solid oxide fuel cells based on Tm-doped SrCeO2-δ semiconductor electrolytes. Mater. Today Energy *20*, 100661.

93. Lund, T.L. (2021). Nano-scale view into solid oxide fuel cell and semiconductor 3 membrane fuel cell: material and technology 4. Perspective *1*, 2.

94. Zhu, B., Mi, Y., Xia, C., Wang, B., Kim, J.-S., Lund, P., and Li, T. (2022). A nanoscale perspective on solid oxide and semiconductor membrane fuel cells: materials and technology. Energy Mater. *1*, 100002.

95. Shah, M.A.K.Y., Rauf, S., Mushtaq, N., Zhu, B., Tayyab, Z., Yousaf, M., Hanif, M.B., Lund, P.D., Lu, Y., and Asghar, M.I. (2021). Novel perovskite semiconductor based on Co/Fe-codoped LBZY (La0. 5Ba0. 5 Co0. 2Fe0. 2Zr0. 3Y0. 3O3− δ) as an electrolyte in ceramic fuel cells. ACS Appl. Energy Mater. *4*, 5798–5808.

96. Shah, M.Y., Lu, Y., Mushtaq, N., Yousaf, M., Rauf, S., Asghar, M.I., Lund, P.D., and Zhu, B. (2022). Perovskite Al-SrTiO 3 semiconductor electrolyte with superionic conduction in ceramic fuel cells. Sustain. Energy Fuels *6*, 3794–3805.

97. Lu, Y., Mi, Y., Li, J., Qi, F., Yan, S., and Dong, W. (2021). Recent progress in semiconductor-ionic conductor nanomaterial as a membrane for low-temperature solid oxide fuel cells. Nanomaterials *11*, 2290.

98. Zhu, B., Fan, L., Mushtaq, N., Raza, R., Sajid, M., Wu, Y., Lin, W., Kim, J.-S., Lund, P.D., and Yun, S. (2021). Semiconductor electrochemistry for clean energy conversion and storage. Electrochem. Energy Rev. *4*, 757–792.

99. Xia, C., Qiao, Z., Shen, L., Liu, X., Cai, Y., Xu, Y., Qiao, J., and Wang, H. (2018). Semiconductor electrolyte for low-operating-temperature solid oxide fuel cell: Li-doped ZnO. Int. J. Hydrogen Energy *43*, 12825–12834.

100. Shah, M.Y., Rauf, S., Mushtaq, N., Tayyab, Z., Ali, N., Yousaf, M., Xing, Y., Akbar, M., Lund, P.D., Yang, C.P., et al. (2020). Semiconductor Fe-doped SrTiO3-δ perovskite electrolyte for low-temperature solid oxide fuel cell (LT-SOFC) operating below 520° C. Int. J. Hydrogen Energy *45*, 14470–14479.

101. Shah, M.A.K.Y., Rauf, S., Zhu, B., Mushtaq, N., Yousaf, M., Lund, P.D., Xia, C., and Asghar, M.I. (2021). Semiconductor Nb-doped SrTiO3− δ perovskite electrolyte for a ceramic fuel cell. ACS Appl. Energy Mater. *4*, 365–375.

102. Dong, W., Tong, Y., Zhu, B., Xiao, H., Wei, L., Huang, C., Wang, B., Wang, X., Kim, J.-S., and Wang, H. (2019). Semiconductor TiO 2 thin film as an electrolyte for fuel cells. J. Mater. Chem. A Mater. *7*, 16728–16734.

103. Zhu, B., Yun, S., and Lund, P.D. (2018). Semiconductor-ionic Materials Could Play an Important Role in Advanced Fuel-to-electricity Conversion (Wiley Online Library).

104. Xia, C., Mi, Y., Wang, B., Lin, B., Chen, G., and Zhu, B. (2019). Shaping triple-conducting semiconductor BaCo0.4Fe0. 4Zr0. 1Y0.1O3-δ into an electrolyte for low-temperature solid oxide fuel cells. Nat. Commun. *10*, 1707–1709.

105. Fan, L., Wang, C., Osamudiamen, O., Raza, R., Singh, M., and Zhu, B. (2012). Mixed ion and electron conductive composites for single component fuel cells: I. Effects of composition and pellet thickness. J. Power Sources *217*, 164–169.

106. Fan, L., Ma, Y., Wang, X., Singh, M., and Zhu, B. (2014). Understanding the electrochemical mechanism of the core–shell ceria–LiZnO nanocomposite in a low temperature solid oxide fuel cell. J. Mater. Chem. A Mater. *2*, 5399–5407.

107. Lund, P.D., Zhu, B., Li, Y., Yun, S., Nasibulin, A.G., Raza, R., Leskelä, M., Ni, M., Wu, Y., Chen, G., et al. (2017). Standardized procedures important for improving single-component ceramic fuel cell technology. ACS Energy Lett. *2*, 2752–2755.

108. Shao, K., Li, F., Zhang, G., Zhang, Q., Maliutina, K., and Fan, L. (2019). Approaching durable single-layer fuel cells: promotion of electroactivity and charge separation via nanoalloy redox exsolution. ACS Appl. Mater. Interfaces *11*, 27924–27933.

109. Zhu, B., Wang, B., Wang, Y., Raza, R., Tan, W., Kim, J.-S., Van Aken, P.A., and Lund, P. (2017). Charge separation and transport in La0.6Sr0. 4Co0.2Fe0. 8O3-δ and ion-doping ceria heterostructure material for new generation fuel cell. Nano Energy *37*, 195–202.

110. Cai, Y., Chen, Y., Akbar, M., Jin, B., Tu, Z., Mushtaq, N., Wang, B., Qu, X., Xia, C., and Huang, Y. (2021). A bulk-heterostructure nanocomposite electrolyte of Ce0.8Sm0. 2O2-δ–SrTiO3 for low-temperature solid oxide fuel cells. Nano-Micro Lett. *13*, 46.

111. Mushtaq, N., Xia, C., Dong, W., Wang, B., Raza, R., Ali, A., Afzal, M., and Zhu, B. (2019). Tuning the energy band structure at interfaces of the SrFe0.75Ti0. 25O3− δ–Sm0. 25Ce0.75O2− δ heterostructure for fast ionic transport. ACS Appl. Mater. Interfaces *11*, 38737–38745.

112. Xing, Y., Zhu, B., Hong, L., Xia, C., Wang, B., Wu, Y., Cai, H., Rauf, S., Huang, J., Asghar, M.I., et al. (2022). Designing high interfacial conduction beyond bulk via engineering the semiconductor–ionic heterostructure CeO2− δ/BaZr0.8Y0. 2O3 for superior proton conductive fuel cell and water electrolysis applications. ACS Appl. Energy Mater. *5*, 15373–15384.

113. Ganesh, K.S., Fan, L., Wang, B., Jeevan Kumar, P., and Zhu, B. (2022). Built-in electric field for efficient charge separation and ionic transport in LiCoO2/SnO2 semiconductor junction fuel cells. ACS Appl. Energy Mater. *5*, 12513–12522.

114. Hossain, M.K., Biswas, M.C., Chanda, R.K., Rubel, M.H.K., Khan, M.I., and Hashizume, K. (2021). A review on experimental and theoretical studies of perovskite barium zirconate proton conductors. Emergent Mater. *4*, 999–1027.

115. Ni, M.F., Wang, X.M., Wang, H.Y., Chang, Y., Huang, X.F., and Zhang, B.W. (2020). Fuel cells that operate at 300 to 500 C. Science *277*, 138–145.

116. Lu, Y., Zhu, B., Shi, J., and Yun, S. (2022). Advanced low-temperature solid oxide fuel cells based on a built-in electric field. Energy Mater. *1*, 100007.

117. Shah, M.Y., Lu, Y., Mushtaq, N., Singh, M., Rauf, S., Yousaf, M., and Zhu, B. (2022). ZnO/MgZnO Heterostructure Membrane with Type II Band Alignment for Ceramic Fuel Cells.